Coupled-channel analysis for ϕ photoproduction with $\Lambda(1520)$

S. Ozaki* and A. Hosaka†
Research Center for Nuclear Physics (RCNP), Osaka University, Ibaraki, Osaka 567-0047, Japan

H. Nagahiro‡
Department of Physics, Nara Women's University, Nara 630-8506, Japan

O. Scholten§
Kernfysisch Versneller Instituut, University of Groningen, NL-9747 AA Groningen, Netherlands
(Received 22 May 2009; published 4 September 2009)

We investigate photoproduction of ϕ mesons off protons within a coupled-channel effective-Lagrangian method which is based on the K-matrix approach. Since the threshold energy of the $K\Lambda(1520)$ channel is close to that of ϕN, the contribution of this channel to ϕ photoproduction near the threshold energy region may give rise to some unexpected structures. In the transition amplitude $K\Lambda(1520) \to \phi N$, the kinematics allows an intermediate kaon to be on-shell. This happens in the energy region where a peak structure has been observed in ϕ photoproduction. In our calculations, the on-shell kaon effect indeed reproduces a peak structure, though with a magnitude that is far too small to explain the observed effect. As a following step, we introduce a nucleon resonance in our model. The coupling of the resonance to the $K\Lambda(1520)$ and ϕN channels is not suppressed by the Okubo-Zweig-Iizuka (OZI) rule if the resonance contains a dominant hidden strangeness component. We find that the resonance can reproduce a peak structure of the correct magnitude at the right energy. We also investigate the effects of coupled channels and the resonance on the angular distribution and the spin-density matrices for ϕ photoproduction.

DOI: 10.1103/PhysRevC.80.035201 PACS number(s): 13.60.Le, 25.20.Lj, 11.55.Jy, 25.75.Dw

I. INTRODUCTION

Photo-induced strangeness production is a main topic in hadron physics. The relevant photon energy of about 1 GeV is still well below the regime of perturbative QCD, and hence one expects large nonperturbative effects. This energy is also well above the energy region that is controlled by low-energy theorems. At the energies for strangeness production, important ingredients are the various baryon resonances and coupled-channel effects.

Recently, several photon facilities have reported interesting results in the energy region of strangeness production, such as pentaquarks [1,2], Λ resonances [3,4], and ϕ-meson production [5–7]. The latter has the unique feature that the gluon dynamics dominates in the reaction process because the process is suppressed by the Okubo-Zweig-Iizuka (OZI) rule thanks to the dominant $\bar{s}s$ structure of the ϕ meson. As shown in Fig. 1, the cross section of ϕ photoproduction increases with increasing energy, which can be explained by a Pomeron and meson exchange model [9,10]. The Pomeron is introduced in Regge theory for high-energy hadron scattering and is considered to be dominated by gluon dynamics. It was also shown that this model reproduces the angular dependence in the diffractive region, spin observables, and the energy dependence [11]. Since Regge theory was developed to describe average properties of high-energy scattering processes, such a good agreement is much better than expected. Extrapolation from the high-energy region predicts a smooth energy dependence of the cross section down to the threshold energy for the reaction. Interestingly, the recent observation at the laser electron photon beamline at SPring-8 (LEPS) strongly indicates a peak structure (solid dots in Fig. 1) at around $E_\gamma(\text{lab}) \sim 2$ GeV. Such a structure is difficult to explain in conventional models of ϕ photoproduction, and it is the subject of the present paper to explore possible explanations for this.

The energy at which the peak structure in the ϕ-photoproduction cross section occurs lies very close to the threshold of $\Lambda(1520)$ production. Since the peak seems to have a rather narrow width, channel coupling to the $\Lambda(1520)$ resonance could be responsible for it. In this paper, we will present an analysis of these data in terms of the Groningen K-matrix model, which is based on an effective Lagrangian formulation for the reaction kernel. This kernel obeys gauge invariance and crossing symmetry and is covariant. All these conditions are conserved in the K-matrix formulation, which in addition imposes the unitarity of the scattering matrix, provided that the kernel is Hermitian. The effective Lagrangian for the kernel is also consistent with chiral symmetry. To investigate whether the observed structures in the ϕ-photoproduction cross section could be due to coupled-channel phenomena in which the $\Lambda(1520)$ resonance is expected to play a crucial role, we extend the Groningen K-matrix approach to include the $\Lambda(1520)$ resonance. We will not consider, however, other channels such as $K^*\Lambda$ and $K^*\Sigma$, since the K^* meson has a larger width than the $\Lambda(1520)$ resonance and the ϕ meson.

In Sec. II A, the basic principles of the Groningen K-matrix approach will be shortly reviewed. For the interaction kernels, we follow previous approaches where possible; for

*sho@rcnp.osaka-u.ac.jp
†hosaka@rcnp.osaka-u.ac.jp
‡nagahiro@rcnp.osaka-u.ac.jp
§scholten@kvi.nl

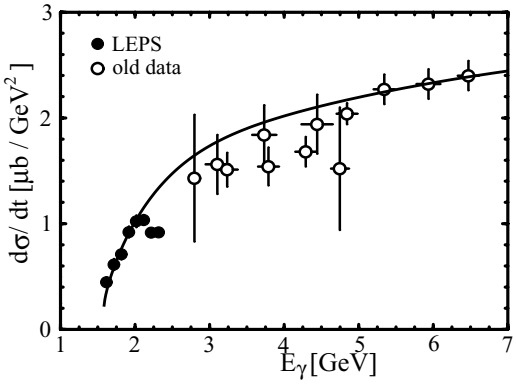

FIG. 1. Differential cross section $d\sigma/dt(\theta = 0)$ as a function of the photon energy E_γ in the laboratory system. The solid line is the sum of Pomeron and meson (π and η) exchange contributions. The data are from Refs. [6,8].

$\gamma N \to \phi N$, the Pomeron and meson exchange model is employed [9,10]; and for $\gamma N \to K\Lambda(1520)$, the effective Lagrangian method is used [12]. The new ingredient introduced here is the $K\Lambda(1520) \to \phi N$ coupling. A brief description of the kernels is given in Secs. II B–II D, while the effective Lagrangians used in these transition amplitudes are presented in Appendix A.

In the attempt to explain the peak structure in the cross section, we pay attention to the following two aspects. One is an on-shell kaon exchange effect in the transition kernel $K\Lambda(1520) \to \phi N$, which is kinematically allowed and which produces a singular structure in the energy region $E_\gamma \sim 2$ GeV. We discuss this effect in Sec. II E. It turns out, however, that the inclusion of the two coupled channels with the above singular behavior cannot explain the observed peak structure in the cross section. As another possibility, we introduce a nucleon resonance as a bare pole in the coupled-channel approach in Sec. II F. We assume that this nucleon resonance contains a large fraction of hidden $s\bar{s}$ or $K\bar{K}$ components, and that such a state will not be produced directly in photon-induced reactions and has a sufficiently large coupling to $K\Lambda(1520)$ as well as to ϕN. In Sec. III, we present results for cross sections, including the t dependence, and spin observables. The role of the on-shell kaon kinematics and nucleon resonances are discussed in detail. The final section is devoted to discussions and a summary.

II. DESCRIPTION OF THE MODEL

Our model calculations are based on a coupled-channel calculation using the K-matrix formulation as described in the following section. We include πN, ρN, ηN, $K\Lambda$, $K\Sigma$, $K\Lambda(1520)$, and ϕN channels. The kernel for our coupled-channel calculation is derived from an effective Lagrangian method. Included are the s-, t-, and u-channel Born diagrams supplemented by the contact terms to ensure gauge invariance where necessary. In addition, a spectrum of low-lying baryonic contributions is included in the s and u channels. A more complete account of the terms in the effective Lagrangians is given in Appendix A.

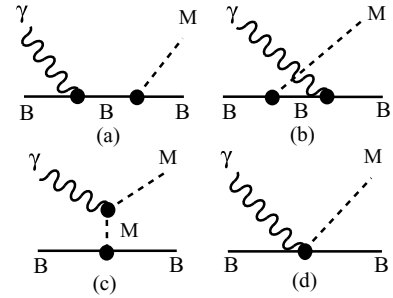

FIG. 2. Feynman diagrams included in this work. First row: s- and u-channel diagrams, the external baryons B in these diagrams are those included in the coupled channels, N, Λ, Σ, $\Lambda(1520)$, and the intermediate ones can also be N^*, Δ resonances in addition to those of the external ones when allowed. M stands for the mesons included in the model space π, η, K, ρ, ϕ. Second row: t-channel contributions with meson exchange π, K, η, K^*, ρ, ω, and the contact term required by the gauge invariance.

A. K-matrix model

The coupled-channel (or rescattering) effects are included in our model via the K-matrix formalism. In this section, we present a short overview of this approach; a more detailed description can be found in Refs. [13–15].

In the K-matrix formalism, the scattering matrix is written as

$$T = \frac{K}{1 - iK}. \tag{1}$$

It is easy to check that the resulting scattering amplitude $S = 1 + 2iT$ is unitary provided that K is Hermitian. The construction in Eq. (1) can be regarded as the resummation of an infinite series of loop diagrams by making a series expansion,

$$T = K + iKK + i^2KKK + \cdots. \tag{2}$$

The product of two K matrices can be rewritten as a sum of different one-loop contributions. However, not the entire spectrum of loop contributions present in a systematic field-theoretical approach is generated in this way, and the missing ones should be accounted for in the kernel. In constructing the kernel, care should be taken to avoid double counting. For this reason, we include in the kernel tree-level diagrams only [Figs. 2(a)–2(c)], modified with form-factors and contact terms [Fig. 2(d)]. The contact terms (or four-point vertices) ensure gauge invariance of the model and express the model dependence introduced by working with form factors (see Appendix A). Contact terms and form factors can be regarded as accounting for loop corrections that are not generated in the K-matrix procedure, or for short-range effects that have been omitted from the interaction Lagrangian. Inclusion of both s- and u-channel diagrams [Figs. 2(a) and 2(b), respectively] in the kernel ensures compliance with crossing symmetry.

B. Kernel $\gamma N \to \phi N$

Because of the OZI rule, the nucleon pole (s- and u-type diagrams) contribution will be suppressed for the $\gamma N \to \phi N$ channel. The same will hold for the nucleon resonance

contributions if they are dominated by u and d quarks. Therefore the t-channel contributions will be the most important in the kernel. We include meson (π,η) exchange diagrams as well as the Pomeron contribution. Effective Lagrangians used in meson exchange amplitudes are presented in Appendix A. As discussed in Sec. III, the kernel is dominated by the Pomeron contribution. According to the recipe of Refs. [9,10,16], the amplitude of the Pomeron exchange is given by

$$\mathcal{M} = \bar{u}(p_{N_f})\mathcal{M}_{\mu\nu}u(p_{N_i})\epsilon_\phi^{*\mu}\epsilon_\gamma^{\nu}, \tag{3}$$

where ϵ_ϕ and ϵ_γ are the polarization vectors of the ϕ meson and photon, and $\mathcal{M}_{\mu\nu}$ is

$$\mathcal{M}^{\mu\nu} = M(s,t)\Gamma^{\mu\nu}. \tag{4}$$

Here the transition operator $\Gamma^{\mu\nu}$ reads

$$\Gamma^{\mu\nu} = \not{k}_\gamma\left(g^{\mu\nu} - \frac{p_\phi^\mu p_\phi^\nu}{p_\phi^2}\right) - \gamma^\nu\left(k_\gamma^\mu - p_\phi^\mu\frac{k_\gamma\cdot p_\phi}{p_\phi^2}\right) - \left(p_\phi^\nu - \frac{\bar{p}^\nu k_\gamma\cdot p_\phi}{\bar{p}\cdot k_\gamma}\right)\left(\gamma^\mu - \frac{\not{p}_\phi p_\phi^\mu}{p_\phi^2}\right),$$

with $\bar{p} = (p_{N_i} + p_{N_f})/2$. This amplitude satisfies gauge invariance. The factor $M(s,t)$ is written as

$$M(s,t) = C_p F_N(t)F_\phi(t)\left(\frac{s}{s_p}\right)^{\alpha_p(t)-1}\exp\left(-\frac{i\pi}{2}\alpha_p(t)\right), \tag{5}$$

where $F_N(t)$ is the isoscalar form factor of the nucleon, and $F_\phi(t)$ is the form factor for the photon-ϕ meson-Pomeron coupling. They are parametrized as

$$F_N(t) = \frac{4M_N^2 - a_N^2 t}{(4M_N^2 - t)(1 - t/t_0)^2},$$

$$F_\phi(t) = \frac{2\mu_0^2}{(1 - t/M_\phi^2)(2\mu_0^2 + M_\phi^2 - t)}.$$

In Eq. (5) the Pomeron trajectory $\alpha_p(t) = 1.08 + 0.25t$ is determined from hadron elastic scattering in the high-energy region. The strength factor C_p is

$$C_p = \frac{6e\beta_s\beta_u}{\gamma_\phi}, \tag{6}$$

where $\gamma_\phi = 6.7$ is the ϕ-meson decay constant. The constants β_s and β_u are Pomeron couplings with the strange quark in a ϕ meson and the light quark in a proton, respectively. For other parameters, we use standard values for the Pomeron exchange model, that is, $t_0 = 0.7$ GeV^2, $\mu_0^2 = 1.1$ GeV^2, $s_P = 4$ GeV^2, $a_N = 2$, and $\beta_s = 1.44$ and $\beta_u = 2.04$ GeV^{-1}.

C. Kernel $\gamma N \to K\Lambda(1520)$

We can expect that the $\gamma N \to K\Lambda(1520)$ channel contributes to ϕ-meson photoproduction through coupled-channel effects near the threshold region because the threshold of this channel is very close to that of the ϕN channel. For $\Lambda(1520)$ photoproduction, we use the model in Ref. [12], which is based on the effective Lagrangian method. The relevant terms of the Lagrangian are presented in Appendix A. In this model, the most important contribution is given by the contact term

$$\mathcal{M}_c = -\frac{eg_{KN\Lambda^*}}{m_K}\bar{u}^\mu\epsilon_\mu\gamma_5 u\cdot F_c, \tag{7}$$

where u^μ and ϵ^μ are the Rarita-Schwinger vector-spinor (see Appendix C) and photon polarization vector, respectively, and F_c is a hadronic form factor (see Appendix A). The coupling constant $g_{KN\Lambda^*} = -11$ [$\Lambda^* \equiv \Lambda(1520)$] is determined by the decay rate of $\Lambda(1520) \to KN$, $\Gamma_{\Lambda(1520)\to KN} \simeq 7$ MeV. Gauge invariance is satisfied when all Born diagrams are summed. This model successfully reproduces the experimental data in the medium-energy region ($3 \leqslant E_\gamma \leqslant 5$ GeV). Recent LEPS data [17] also support this model in the low-energy region.

D. Kernel $K\Lambda(1520) \to \phi N$

For the terms in the effective interaction Lagrangian for the $K\Lambda(1520) \to \phi N$ kernel, which plays a crucial role in coupled-channel effects, we choose

$$\mathcal{L}_{KN\Lambda^*} = i\frac{g_{KN\Lambda^*}}{m_K M_{\Lambda^*}}\bar{N}\gamma_5[(\partial_\alpha K^+)(\not{\partial}\Lambda^{*\alpha}) - (\partial_\mu K^+)\gamma_\alpha(\partial^\mu\Lambda^{*\alpha})], \tag{8}$$

$$\mathcal{L}_{\phi KK} = -ig_\phi(\partial^\mu K^- K^+ - \partial^\mu K^+ K^-)\phi_\mu, \tag{9}$$

$$\mathcal{L}_{\phi\Lambda^*\Lambda^*} = -\frac{g_\phi}{M_{\Lambda^*}^2}(\partial^\rho\bar{\Lambda}^{*\beta})[g_{\alpha\beta}g_{\rho\tau} - g_{\tau\beta}g_{\rho\alpha}] \times\left(-\gamma_\mu + \frac{\kappa_\phi}{2M_{\Lambda^*}}\sigma_{\mu\nu}\partial^\nu\right)\phi^\mu(\partial^\tau\Lambda^{*\alpha}), \tag{10}$$

where we assume universality for ϕ-meson and hadron couplings including strangeness, that is, $g_\phi = g_{\phi KK}$. The vertices are chosen such that the coupling to the spin-1/2 component of the intermediate Rarita-Schwinger propagator vanishes (so-called gauge-invariant vertices). From the decay width $\Gamma_{\phi\to KK}$ we obtain the value $|g_\phi| = 4.7$. For simplicity, we take $\kappa_\phi = 0$. Here we employ these Lagrangians rather than those similar to Eqs. (A5) and (A6) with the photon field A_μ replaced by ϕ_μ, since for coupling to the photon field, the magnetic coupling (set to zero for ϕ-meson production) is dominant together with the associated contact term. For coupled-channel calculations, a proper treatment of off-shell properties is important and the choice of Eqs. (8)–(10) is one way to reduce the ambiguities in the off-shell propagator of a spin-3/2 particle. Replacing the derivative in Eq. (8) by a covariant derivative, that is, $\partial_\mu K^+ \to (\partial_\mu - ig_\phi\phi_\mu)K^+$ (the minus sign is due to $Q_s = -1$ in the case of K^+) and $\partial_\mu\Lambda^* \to (\partial_\mu + ig_\phi\phi_\mu)\Lambda^*$ (the plus sign is due to $Q_s = +1$ in the case of Λ^*), we obtain the contact term

$$\mathcal{L}_{\phi KN\Lambda^*} = -\frac{g_\phi g_{KN\Lambda^*}}{m_K M_{\Lambda^*}}\bar{N}\gamma_5 \times[-\phi_\alpha K^+\not{\partial}\Lambda^{*\alpha} + \partial_\alpha K^+\gamma_\mu\phi^\mu\Lambda^{*\alpha}]. \tag{11}$$

Here we find an additional term, the second term of Eq. (11), which does not exist in Eq. (A7) for on-shell Λ^*. This term, however, is shown to be suppressed by the order $O(p/M)$ and has a negligible contribution to the scattering amplitude. Using these effective interaction Lagrangians, we obtain the

transition amplitudes $K\Lambda(1520) \to \phi N$

$$\mathcal{M}_u = i\frac{g_\phi g_{KN\Lambda^*}}{m_K M_{\Lambda^*}^3}\bar{u}(p_N)\gamma_5[p_{K\nu}\not{q}_u - (p_K\cdot q_u)\gamma_\nu] \times D_{3/2}^{\nu\beta}[g_{\alpha\beta}(q_u\cdot p_{\Lambda^*}) - p_{\Lambda^*\beta}q_{u\alpha}]\not{\epsilon}_\phi u^\alpha(p_{\Lambda^*}), \quad (12)$$

$$\mathcal{M}_t = -\frac{g_\phi g_{KN\Lambda^*}}{m_K}\frac{1}{q_t^2 - m_K^2}(q_t - p_K) \cdot\epsilon_\phi\bar{u}(p_N)\gamma_5(q_t\cdot u(p_{\Lambda^*})), \quad (13)$$

$$\mathcal{M}_c = \frac{g_\phi g_{KN\Lambda^*}}{m_K M_{\Lambda^*}}\bar{u}(p_N)\gamma_5(\not{p}_{\Lambda^*}\not{\epsilon}_{\phi\alpha} - \not{\epsilon}_\phi p_{K\alpha})u^\alpha(p_{\Lambda^*}), \quad (14)$$

where the four-momenta of the kaon, Λ^*, ϕ, and N are denoted by p_K, p_{Λ^*}, p_ϕ, and p_N, respectively; we have defined $q_t = p_\phi - p_K$, and ϵ_ϕ^μ is the polarization vector of the ϕ meson. $D_{3/2}^{\alpha\beta}$ stands for the spin-3/2 propagator

$$D_{3/2}^{\alpha\beta}(q_u) = -i\frac{\not{q}_u + M_{\Lambda^*}}{q^2 - M_{\Lambda^*}^2}\left[g^{\alpha\beta} - \frac{1}{3}\gamma^\alpha\gamma^\beta - \frac{2}{3M_{\Lambda^*}^2}q_u^\alpha q_u^\beta - \frac{q_u^\alpha\gamma^\beta - q_u^\beta\gamma^\alpha}{3M_{\Lambda^*}}\right], \quad (15)$$

where $q_u = p_{\Lambda^*} - p_\phi$. Assuming $g_{\phi NN} = 0$, as suggested by the OZI rule, the s-channel amplitude vanishes.

E. On-shell kaon exchange

In the t-channel contribution to the $K\Lambda(1520) \to \phi N$ kernel, (Fig. 3), the exchanged kaon can reach the on-shell pole for certain kinematical conditions. The on-shell condition is

$$t(W(E_\gamma), \cos\theta_K) - m_K^2 = 0, \quad (16)$$

where t is the momentum transfer as a function of the invariant mass W, which in turn depends on the energy of the in-coming photon in the $\gamma N \to \phi N$ channel and on $\cos\theta_K$, where θ_K is the angle between the out-going ϕ meson and the in-coming kaon, as shown in Fig. 3. Therefore, Eq. (16) gives a relation between E_γ and $\cos\theta_K$, which is shown by the solid line in Fig. 4(a). Since $|\cos\theta_K| \leqslant 1$, the solution of Eq. (16) is kinematically limited to a narrow energy region given by the photon energy $1.7 \lesssim E_\gamma \lesssim 2.1$ GeV. In Fig. 4(a), the allowed region is colored in blue. An interesting point is that the blue region $E_\gamma \lesssim 2.1$ GeV corresponds to the region in which the peak structure in the production cross section is observed, as shown in Fig. 4(b).

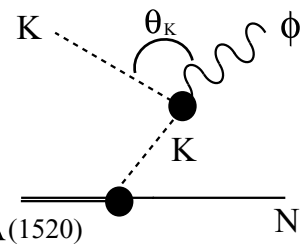

FIG. 3. t-channel diagram in the kernel $K\Lambda(1520) \to \phi N$.

The fact that the intermediate kaon may become on-shell is similar to the threshold effect in the coupled-channel dynamics and might be responsible for a singular behavior in the kinematically allowed region.

In reality, this pole contribution is washed out because the $\Lambda(1520)$ resonance as well as the ϕ meson are unstable particles. If they were stable, they could not couple to the on-shell $K\bar{K}N$ intermediate state. The resulting small but finite width of these particles is, however, not yet taken into account in the calculations. This width can be folded with the divergent pole contribution, creating a resonance-like structure for the matrix element. To simulate this, we introduce an effective width for the exchanged kaon reflecting the decay width of the external ϕ meson and the $\Lambda(1520)$ resonance,

$$\frac{i}{t - m_K^2} \to \frac{i}{t - m_K^2 - im_K\Gamma_K}. \quad (17)$$

In Appendix B, we give an estimate for the value of the effective width for the intermediate kaon. We have obtained a value for Γ_K of

$$\Gamma_K > 7.79 \text{ MeV}, \quad (18)$$

in the on-shell region (see Appendix B). In the calculations, we have chosen the value $\Gamma_K = 10$ MeV. In Sec. III, we will discuss the dependence of the calculated ϕ-photoproduction cross section on Γ_K, which is rather small.

F. Nucleon resonance with large $s\bar{s}$ components

In these discussions we have not yet considered any nucleon resonance contributions. A normal nucleon resonance will not contribute to the $K\Lambda(1520) \to \phi N$ kernel because of the OZI rule; however, if the resonance contains a hidden $s\bar{s}$ component, it may strongly couple to ϕN and/or $K\Lambda(1520)$ states and will contribute through the s-channel process. In this paper, as one possibility, we introduce such a nucleon resonance as a pole term, since in the K-matrix approach, resonances are not generated dynamically. This pole term, with the bare mass M_{N^*}, is introduced in the kernels of $K\Lambda(1520) \to K\Lambda(1520)$, $K\Lambda(1520) \to \phi N$, and $\phi N \to \phi N$. This resonance can thus be regarded as a ϕN, $K\Lambda(1520)$, or a $K\bar{K}N$ quasi-bound state or a superposition of such states. The possibility of such a resonance is discussed for a slightly lower energy region in Refs. [19,20]. In contrast to the mass, its finite decay width is dynamically generated through the coupling to the $K\Lambda(1520)$ and ϕN channels. Furthermore, we assume that the resonance is not directly excited in photoproduction. In spite of this, it may contribute to ϕ-meson photoproduction through coupled-channel effects as investigated in this work. Since we do not know the spin and parity of the resonance, we assume $J^P = 1/2^\pm$, for simplicity. The kernels in which the nucleon resonance appears in the s channel are given by

$$\mathcal{M}_{\phi N\to K\Lambda^*}^{N^*} = -i\frac{g_{K\Lambda^*N^*}}{m_K}\frac{g_\phi\kappa_{\phi NN^*}}{4M_N}\bar{u}(p_N)[\not{\epsilon}_\phi\not{p}_\phi - \not{p}_\phi\not{\epsilon}_\phi] \times\Gamma_1\frac{i}{\not{p}_{N^*} - M_{N^*}}\Gamma_2 p_{K\mu}u^\mu(p_{\Lambda^*}), \quad (19)$$

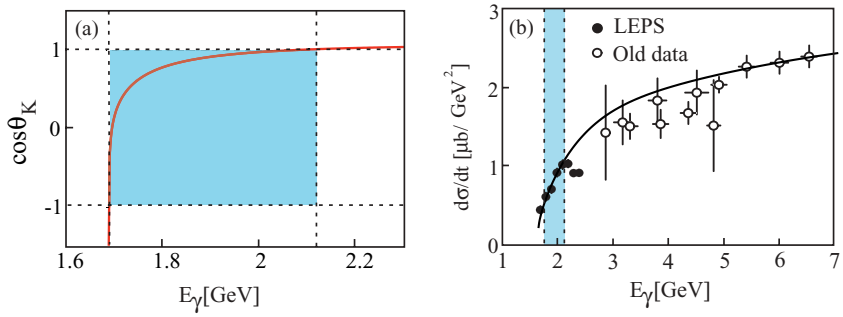

FIG. 4. (Color online) (a) Solution to the on-shell condition of the intermediate kaon. The kinematically allowed region, $-1 \leqslant \cos\theta_K \leqslant 1$ or equivalently $1.7 \leqslant E_\gamma \leqslant 2.1$ GeV is colored blue with the boundary shown by the dashed lines. (b) Allowed region in E_γ is also shown in the plot of the cross section.

$$\mathcal{M}^{N^*}_{K\Lambda^*\to K\Lambda^*} = i\left(\frac{g_{K\Lambda^*N^*}}{m_K}\right)^2 \bar{u}^\mu(p'_{\Lambda^*})p'_{K\mu} \times \Gamma_2 \frac{i}{\not{p}_{N^*} - M_{N^*}}\Gamma_2 p_{K\nu}u^\nu(p_{\Lambda^*}), \quad (20)$$

$$\mathcal{M}^{N^*}_{\phi N\to\phi N} = \left(\frac{g_\phi \kappa_{\phi NN^*}}{4M_N}\right)^2 \bar{u}(p'_N)[\not{\epsilon}'_\phi \not{p}'_\phi - \not{\epsilon}'_\phi \not{p}'_\phi] \times \Gamma_1 \frac{i}{\not{p}_{N^*} - M_{N^*}}\Gamma_1[\not{\epsilon}_\phi \not{p}_\phi - \not{\epsilon}_\phi \not{p}_\phi]u(p_N), \quad (21)$$

where $g_{K\Lambda^*N^*}, \kappa_{\phi NN^*}$, and M_{N^*} are free parameters that characterize the N^* resonance. Γ_1 (Γ_2) equals $1_{4\times4}$ (γ_5) for the positive-parity resonance and equals γ_5 ($1_{4\times4}$) for negative-parity resonance.

In the following section, we investigate the extent to which such an N^* resonance with hidden strangeness can be responsible for the peak structure observed in ϕ photoproduction.

III. RESULTS AND DISCUSSIONS

In this section, we present our numerical results for the reaction cross section of $\gamma N \to \phi N$. To investigate the roles of coupled channels, we first discuss the contributions of the different channels. Next we introduce the N^* resonance with hidden strangeness in our model. Finally we show our results for the t dependence of the cross section and spin-density matrices.

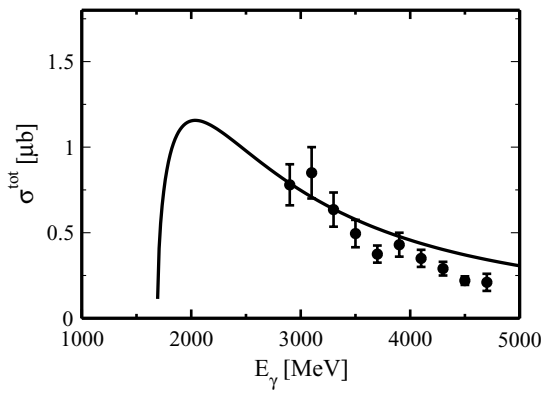

FIG. 5. Total cross section for $\gamma p \to K^+\Lambda(1520)$ as function of the photon energy in the laboratory system E_γ, calculated with a cutoff of $\Lambda_c = 0.7$ GeV. The data are from Ref. [18].

A. Kernel $\gamma N \to K\Lambda(1520)$

As mentioned before, one potentially interesting coupled-channel contribution to ϕ-meson photoproduction is the one going via the $K\Lambda(1520)$ intermediate channel. The reason is that the threshold for this channel lies close to that of ϕN. The magnitude of this coupled-channel contribution is determined by the product of kernels for $\gamma N \to K\Lambda(1520)$ and $K\Lambda(1520) \to \phi N$.

To fix the magnitude of the $\gamma N \to K\Lambda(1520)$ kernel, we compare the calculated cross section for this reaction with data in Fig. 5. The calculated cross sections depend strongly on the cutoff parameter in the hadronic form factor (see Appendix A). Following Ref. [12], a good agreement with the data in the medium-energy region ($3000 \leqslant E_\gamma \leqslant 5000$ MeV) is obtained using a value of $\Lambda_c = 0.7$ GeV. At higher energies, the calculation overestimates the data, however, this is outside the region of interest for the present investigation. Care should be taken when using the parameters of Ref. [12] for the reaction of $\gamma N \to K\Lambda(1520)$ since coupled-channel effects will contribute. Our strategy is first to fix each kernel to reproduce the corresponding data if available and to introduce the coupled-channel effects afterward. If the latter effect is important, we will reconsider the kernels themselves such that the coupled-channel results will reproduce the data. For the $K\Lambda(1520)$ photoproduction, we have found that the coupled effects are not very important.

B. Kernel $K\Lambda(1520) \to \phi N$

The $K\Lambda(1520) \to \phi N$ kernel is one of the most important ingredients in the present coupled-channel analysis. In Fig. 6, various contributions to the differential cross section of the ϕ photoproduction, $d\sigma/dt(\theta = 0)$ are shown when only the $K\Lambda(1520) \to \phi N$ term is included in the kernel to highlight the effect of the coupled channels of $K\Lambda(1520)$ and ϕN. In this case, for example, the lowest order process is given by $\gamma N \to K\Lambda(1520) \to \phi N$.

An important aspect of the kernel for the $K\Lambda(1520) \to \phi N$ channel is the pole in the t-channel kaon that can be hit for certain kinematics. In Sec. II E, we argued that this singularity could be treated effectively by assigning a finite width Γ_K to the intermediate kaon propagator, where we related the width to the physical decay widths of the $\Lambda(1520)$ resonance and ϕ meson in the in-coming and out-going channels. To test the importance of the width attributed to the intermediate kaon we have calculated the cross section for different values

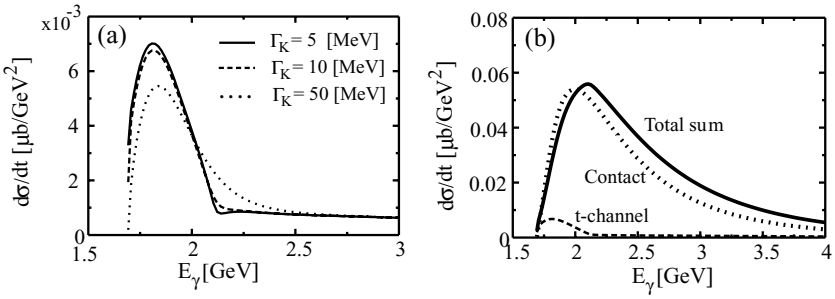

FIG. 6. Differential cross sections of $\gamma N \to \phi N$ at zero degrees, $d\sigma/dt(\theta = 0)$. (a) Effects of changing the width of the intermediate kaon, $\Gamma_K = 5$ MeV (solid line), $\Gamma_K = 10$ MeV (dashed line), and $\Gamma_K = 50$ MeV (dotted line), in a calculation in which only the t-channel kaon exchange contribution is included for the $K\Lambda(1520) \to \phi N$ matrix elements. (b) Result including the full matrix element (solid line), only the contact term (dotted line), and only the t-channel kaon exchange contribution (dashed line).

of Γ_K. In Fig. 6(a), we plot $d\sigma/dt(\theta = 0)$ when only the t-channel contribution of kaon exchange is included in the kernel $K\Lambda(1520) \to \phi N$. Different lines correspond to those calculated for Γ_K values of 5, 10, and 50 MeV. Variation of Γ_K does not influence the result very much, as shown in the figure. Based on the decay width of the ϕ meson and that of the $\Lambda(1520)$ resonance, one expects $\Gamma_K \approx 10$ MeV as argued in the previous section. Therefore, we will use this value in the following calculations.

Interestingly, the cross section in Fig. 6(a) shows a peak structure in the same energy region as the experimental data. However, the magnitude of the peak in the calculation is very small. The effects of the other contributions of the $K\Lambda(1520) \to \phi N$ kernel from the u channel and contact term are investigated in Fig. 6(b), where we can see that the dominant contribution is generated by the contact term (dotted line), which is compared with the case including all terms (solid line). This is similar in structure to that in the $\gamma N \to K\Lambda(1520)$ channel [12]. The t-channel kaon exchange contribution (dashed line) is thus buried under the contribution from the contact term. The u-channel contribution is also negligibly small.

We have also investigated the cutoff dependence of the kernel. In Fig. 7, the solid line is for $\Lambda_c^2 = 0.49$ GeV^2 ($\Lambda_c = 0.7$ GeV), corresponding to the solid line in Fig. 6(b), the dashed line for $\Lambda_c^2 = 0.8$ GeV^2, and the dotted line for $\Lambda_c^2 = 1.2$ GeV^2, which is the value used for other kernels such

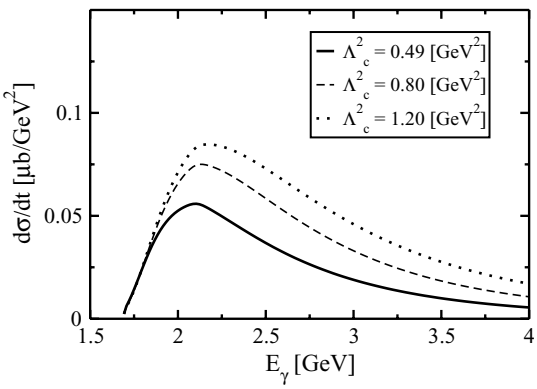

FIG. 7. Differential cross sections for ϕ-meson photoproduction at zero degrees for different values of cut-off parameters in the kernel for $K\Lambda(1520) \to \phi N$, $\Lambda_c^2 = 0.49$, 0.80, and 1.20 GeV^2 for the solid, dashed, and dotted lines, respectively.

$\gamma N \to K\Lambda(1116)$, $\gamma N \to K\Sigma(1193)$, etc. From the figure, we see that the cutoff dependence is not very strong.

One important conclusion that should be drawn from the results presented here is that the cross section calculated by including only the Born terms in the kernel $K\Lambda(1520) \to \phi N$ is not very large by itself, typically, $d\sigma/dt(\theta = 0) \leqslant 0.1\ \mu$b/GeV^2 which is smaller than the experimental values of order 1 μb/GeV^2. However, when other dominant terms especially from the Pomeron exchange term are included, the interference among those terms becomes sizable, as we will see in the following sections.

C. Differential cross section at $\theta = 0$

The dominant contribution to the ϕ-photoproduction cross section is derived from the Pomeron exchange diagram. The magnitude of the Pomeron contribution is fixed by the measured cross section for $E_\gamma \gtrsim 3$ GeV. As shown in Ref. [10], other hadronic contributions such as σ, π, and η exchange diagrams are orders of magnitude smaller at higher photon energies.

In our model, the value of the cutoff parameter in the hadronic form factor is treated as a free parameter as well as the sign of g_ϕ. The hadronic form factor is discussed in more detail in Appendix A. We have calculated the differential cross section for the two cases $g_\phi = +4.7$ and $g_\phi = -4.7$. The absolute value is determined by the ϕ-meson decay width. In Fig. 8, we show the differential cross section calculated in our coupled-channel approach at $\theta = 0$, $d\sigma/dt(\theta = 0)$ as a function of the photon energy in the laboratory fame E_γ. As explained previously, we have included as coupled channels not only the $\Lambda(1520)$ but also those containing the ground state hyperons. As we have anticipated, the main contribution is due to the Pomeron exchange. The most important coupled-channel effect is mainly from the $K\Lambda(1520)$, where the interference of the amplitude of the Pomeron exchange and the coupled channel $K\Lambda(1520)$ is sizable. Other coupled-channel effects, i.e., those from the ground state hyperons, are not significant. In Fig. 8, the thin upper line is for the result of the Pomeron exchange without the coupled channels, and the other two thick lines are for those with the coupled channels for $g_\phi = +4.7$ and $g_\phi = -4.7$, as indicated by the arrows. However, as mentioned in the previous section, the on-shell kaon effect does not reproduce the peak structure with sufficient strength near the threshold region.

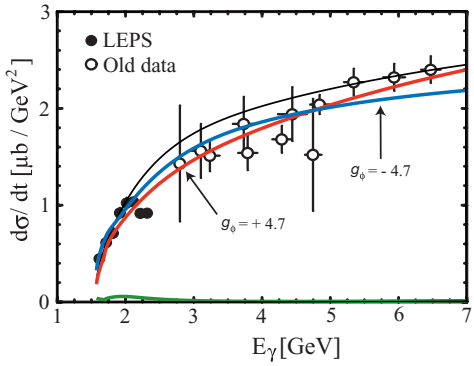

FIG. 8. (Color online) Differential ϕ-meson photoproduction cross section at zero degrees. The topmost black curve shows the results of the tree-level calculation, including the Pomeron contribution. The arrows indicate the curves showing the full coupled-channel results with $g_\phi = +4.7$ and $g_\phi = -4.7$. The lowest line is the effect of only coupled-channel effects, including the $K\Lambda(1520)$ channel and all others.

The Pomeron contribution whose strength is determined by the cross sections beyond $E_\gamma \geqslant 3$ GeV can be smoothly extrapolated downward of the threshold energy region, where it traces the peak value at $E_\gamma \approx 2$ GeV. In this case, the structure at around $E_\gamma \approx 2$ GeV can rather be interpreted as a dip at around $E_\gamma \approx 2.3$ GeV. The structure of either peak or dip can be realized by different phases of amplitude through interference. We have partly tested this already by changing the sign of g_ϕ, which changes the sign of the kernel of such as $K\Lambda(1520) \to \phi N$, $K\Lambda(1116) \to \phi N$, and $K\Sigma(1193) \to \phi N$. As shown in Fig. 8, we could not reproduce the peak/dip structure by the interference in the coupled-channel approach.

D. Introduction of the N^* resonance with large $s\bar{s}$ components

In the previous section, we observed that the peak at around 2 GeV looks rather like a dip around 2.3 GeV after a global fit of the Pomeron exchange amplitude to the experimental data. For this reason, we refer to it as the dip structure rather than the peak structure in the following discussions. To reproduce the observed dip structure in the ϕ-meson photoproduction cross section at forward angle, we will introduce in this section an N^* resonance with large $s\bar{s}$ components, as discussed in Sec. II F. We introduce the resonance as a pole term of mass M_{N^*}. The decay width is then generated dynamically after the coupled-channel equation is solved, and it is related to the coupling strength of the pole term to the ϕN and $K\Lambda(1520)$ channels. The strengths are treated as parameters in order to reproduce the depth and width of the dip. For simplicity, we limited ourselves only to a spin-1/2 resonance. We found that an excellent fit to the data could be obtained by assuming a negative parity resonance, much better so than for a positive resonance. This is due to the interference of the partial waves naturally entering in the calculation with those of the N^* resonance. For instance, the relative motion of the ϕN channel which is coupled to the $J^P = 1/2^-$ partial wave can be an S wave, while for a $J^P = 1/2^+$ it should be a P wave. In the present treatment of the resonance, where the coupling to the channels generates the decay width, the magnitude of the width, energy dependence, and the resulting interference pattern with the other amplitude depend on the spin and parity of the resonance in a complicated manner.

TABLE I. Resonance parameters.

Sets	g_ϕ	$g_{K\Lambda(1520)R}$	$\kappa_{\phi NR}$	M_R (GeV)
A	+4.7	−4.24	0.07	2.25
B	−4.7	−4.90	0.06	2.26

In the following, we will present results for a resonance with $J^P = 1/2^-$. For coupling parameters we have adopted the values as given in Table I where two parameter sets, A and B, are given, corresponding to two signs for g_ϕ, i.e., $g_\phi = +4.7$ (set A) and $g_\phi = -4.7$ (set B). In Fig. 9, sets A and B can both reproduce the dip structure through a destructive interference. The central point of the dip corresponds roughly to the pole position of the resonance when the width of the resonance is not too wide. The width of the resonance can be estimated from the extension of the dip in the cross section shown in Fig. 9 to be around 100 MeV for both parameter sets A and B. An experiment with photon energies $E_\gamma \sim 2.25$ GeV and beyond will be able to provide more information on resonance parameters.

E. t dependence

In this section, we discuss the t dependence of the cross section. In Fig. 10, theoretical results for $d\sigma/dt(\theta = 0)$ with and without coupled channels are compared with the LEPS data [6]. At forward angles, the differences between the tree-level and the coupled-channel results are not very large. In the backward region, however, there are large differences. This is because coupled-channel effects tend to enhance the cross section at large angles. The effect is then further enlarged by the inclusion of the N^* resonance. Similar effects are also seen in ρ-meson photoproduction, where coupled-channel effects

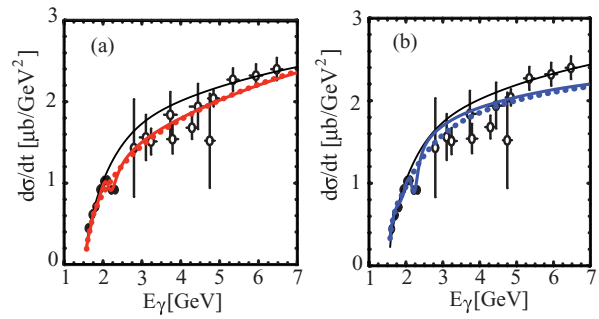

FIG. 9. (Color online) Effect of a spin-$1/2^-$ N^* resonance on the forward angle ϕ-meson photoproduction cross section. The thin black line in the both figures are tree-level results. The thick solid lines in (a) and (b) show the results of sets A and B, respectively. The dotted lines in both figures denote the results of the coupled-channel calculations without the resonance as corresponding to the solid lines in Fig. 8.

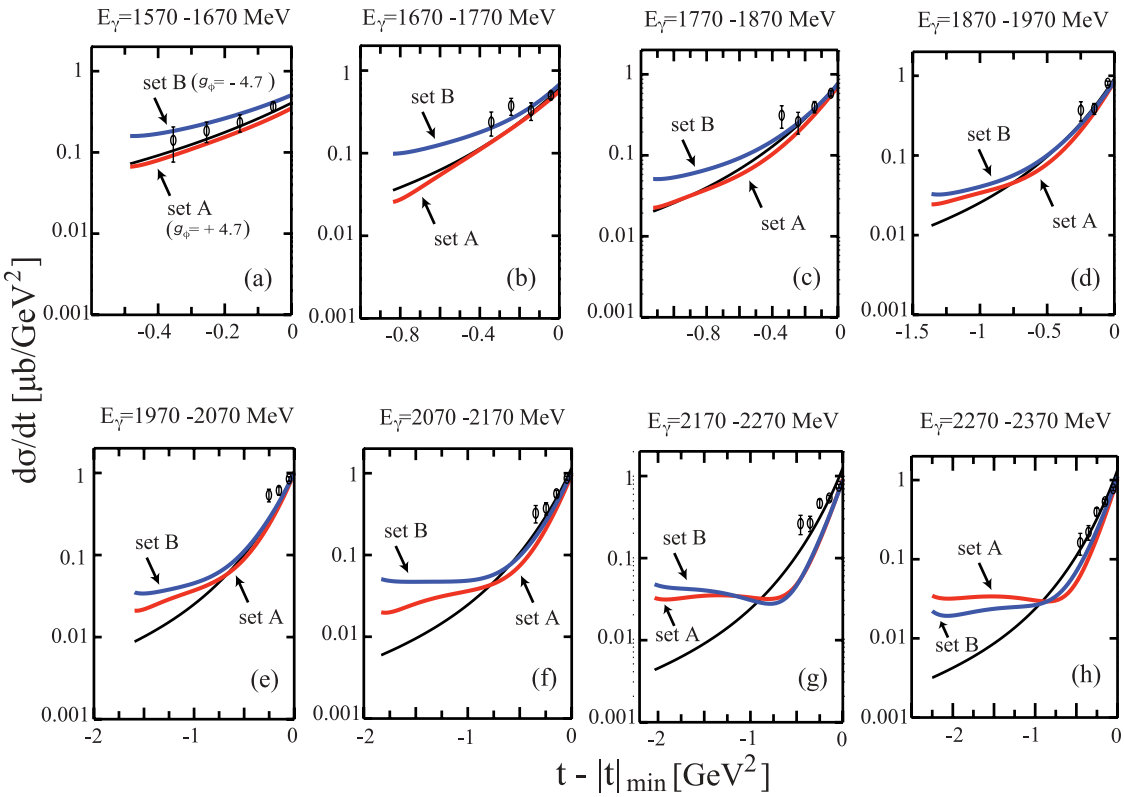

FIG. 10. (Color online) t dependence of the cross section at various photon energies E_γ as indicated above each panel. The black line is the tree-level result; arrows mark the other lines as results of sets A and B. The data are from Ref. [6].

successfully reproduce the observed cross section at backward angles [21]. In our present calculation, the N^* resonance has an important contribution such that the enhancement at large angle is more prominent in the resonance energy region.

In the present calculation, the forward angle structure is dominated by the Pomeron exchange, while at the backward angles the dominant contribution is caused by coupled-channel effects with the nucleon resonance N^*. In many other hadronic reactions at energies well above 2 GeV, one sees that the cross section at forward angles can be explained quite accurately by Reggeon exchange [22–25], while at backward angles more complicated processes contribute.

F. Spin-density matrix

In general, spin observables provide a sensitive test of the reaction mechanism. We have therefore calculated these quantities to investigate the coupled-channel effects. Following Refs. [11,26], we have calculated the spin-density matrices in the Gottfried-Jackson (GJ) system. In the LEPS experiment, measurements were made for $t + |t|_{\rm min} > -0.2$ GeV^2. To obtain the spin-density matrices for a similar kinematics as for the LEPS experiment, we performed our calculation at an angle of $\theta = 20^\circ$.

Figure 11(a) shows ρ^0_{00}, which is related to the single spin-flip amplitude in the GJ system. At the tree level, only the Pomeron exchange can contribute to ρ^0_{00}, whereas the meson exchange contributions vanish exactly. The coupled-channel effects are large, as can be seen from the figure. There is a wide structure in the energy region of $E_\gamma \simeq 1.8$ (set A) and 2 GeV (set B), and also a very narrow dip at the low energy $E_\gamma \sim 1.7$ GeV. This dip structure is due to the contribution from the on-shell kaon in the $K\Lambda(1520) \to \phi N$ channel. Since the non-spin-flip amplitude gives the dominant contribution to the cross section at forward angles, the coupled-channel effects can be much more pronounced in the spin-flip amplitude. The N^* resonance gives only a minor contribution to ρ^0_{00}, as shown by a tiny bump at $E_\gamma \sim 2.25$ GeV.

Figure 11(b) shows ρ^0_{1-1}, which is related to the double spin-flip amplitude in the GJ frame. Only the Pomeron exchange contributes to this spin-density matrix at the tree level since meson exchanges cannot transfer spin 2 if they have spin less than 2, and their contributions thus vanish. The coupled-channel effects are very important especially for the t-channel contribution of the $K\Lambda(1520) \to \phi N$ amplitude. We see either a dip (set A) or peak (set B) structure in the low-energy region due to the on-shell kaon effect. These effects are larger than the Pomeron contribution in the low-energy region. The contribution due to the N^* resonance is small. Our calculation, however, does not reproduce the data, as shown in Fig. 11(b). From the figures of ρ^0_{00} and ρ^0_{1-1}, we emphasize that higher order perturbation effects are important for spin observables. A similar conclusion is reached in Ref. [27].

Figure 11(c) shows ρ^1_{1-1}, which is related to the asymmetry due to the interference of natural (Pomeron) and unnatural (π,η) parity t-channel exchanges. In this matrix element, the

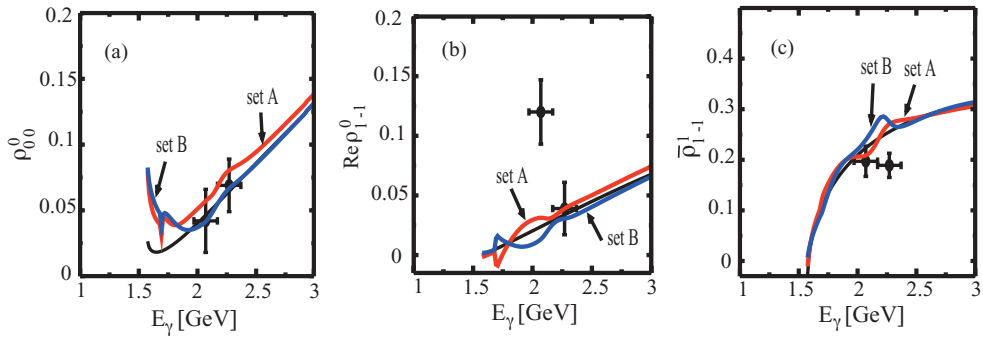

FIG. 11. (Color online) Spin-density matrix for ϕ-meson photoproduction as a function of the photon energy in the GJ system, (a) ρ^0_{00}, (b) ρ^0_{1-1}, (c) ρ^1_{1-1}. In the calculation, the ϕ-meson angle is fixed at $\theta = 20^\circ$. The black line is the tree-level results; the other lines are results of sets A and B. The data are from Ref. [6].

non-spin-flip amplitude is dominant. The coupled-channel effect is small in ρ^1_{1-1} because of the dominance of the Pomeron contribution. There is, however, a visible contribution due to the N^* resonance.

IV. CONCLUSIONS

We have investigated ϕ-meson photoproduction motivated by the recent experimental observation of a peak/dip structure near the threshold region. Our method is based on a coupled-channel K-matrix approach. The kernel used in the K-matrix is constructed based on an effective Lagrangian respecting the symmetries of QCD. In the present work, we have focused on the role of the $K\Lambda(1520)$ reaction channel in coupled-channel calculations because the threshold value of the channel is close to that of the ϕN channel. Additional interest in this channel comes from the fact that in the t-channel contribution to the transition amplitude $K\Lambda(1520) \to \phi N$, the exchanged kaon can be in the on-shell state in the energy region where a distinct structure is observed in ϕ-meson photoproduction. The coupled-channel effect driven by this t-channel contribution itself produces a peak structure in the correct energy region. The dominant contribution to the ϕ-meson photoproduction amplitude, however, is generated by the Pomeron, compared to which the coupled-channel effect induced by the t-channel in the $K\Lambda(1520) \to \phi N$ transition amplitude is insignificant.

As an alternative explanation for the observed structures, we have considered the effect of an N^* resonance. If the resonance contains a hidden $s\bar{s}$ component [as would be the case for a ϕN or a $K\Lambda(1520)$ molecular state], it should have a large coupling to the $K\Lambda(1520)$ and the ϕN reaction channels. For simplicity, we considered only the case of a spin-1/2 resonance. We found that destructive interference between the tree-level amplitude and the resonance coupled-channel contribution can produce a dip structure which is in excellent agreement with the experimental data. These results suggest the existence of an N^*, $J^P = 1/2^-$ resonance with a mass of 2250 MeV and width of about 100 MeV that has a large $s\bar{s}$ component.

To complete our calculations, we have also presented our results for the t dependence of the ϕ-meson photoproduction cross section and the forward-angle spin-density matrices. In the cross section, the coupled-channel effects are most prominent at backward angles, while they do contribute to certain polarization observables at forward angles. The t dependence at large momentum transfer is perhaps one clear-cut signal of the N^* resonance as well as the dip structure, and therefore it would be interesting if further comparison with experimental data were available.

ACKNOWLEDGMENTS

We thank H. Toki, T. Nakano, S. Titov, and T. Mibe for useful discussions. S.O. acknowledges the International Training Program of Osaka University (sponsored by JSPS) and a visitors grant from the Dutch Organization for Scientific Research (NWO) during his stay at KVI. A.H. is supported in part by the Grant for Scientific Research [(C) No. 19540297] from the Ministry of Education, Culture, Science and Technology (MEXT) of Japan.

APPENDIX A: EFFECTIVE LAGRANGIANS AND FORM FACTORS

In the transition amplitude for $\gamma N \to \phi N$, we calculate the pseudoscalar meson exchange amplitudes in terms of the effective Lagrangians [10]

$$\mathcal{L}_{\gamma\varphi\phi} = \frac{e g_{\gamma\varphi\phi}}{m_\varphi} \epsilon^{\mu\nu\alpha\beta} \partial_\mu \phi_\nu \partial_\alpha A_\beta \varphi, \tag{A1}$$

$$\mathcal{L}_{\varphi NN} = \frac{g_{\varphi NN}}{2M_N} \bar{N} \gamma_\mu \gamma_5 N \partial^\mu \varphi, \tag{A2}$$

where φ stands for the pseudoscalar mesons (π, η).

We calculate the transition amplitudes for $\gamma N \to K\Lambda(1520)$ in terms of the effective Lagrangians [12]

$$\mathcal{L}_{\gamma NN} = -e\bar{N}\left(\gamma^\mu - \frac{\kappa_N}{2M_N}\sigma^{\mu\nu}\partial_\nu\right) N A_\mu, \tag{A3}$$

$$\mathcal{L}_{\gamma KK} = -ie(\partial^\mu K^+ K^- - \partial^\mu K^- K^+) A_\mu, \tag{A4}$$

$$\mathcal{L}_{\gamma\Lambda^*\Lambda^*} = -\frac{\kappa_{\Lambda^*}}{2M_{\Lambda^*}} \bar{\Lambda}^{*\mu} \not{k} \gamma_5 A \Lambda^*_\mu, \tag{A5}$$

TABLE II. Coupling constants.

$g_{\gamma\pi\phi}$	-0.141	$g_{\gamma\eta\phi}$	-0.707
$g_{\pi NN}$	13	$g_{\eta NN}$	1.94
κ_{Λ^*}	0.5	$g_{KN\Lambda^*}$	-11

$$\mathcal{L}_{KN\Lambda^*} = \frac{g_{KN\Lambda^*}}{m_K}\bar{N}\gamma_5\partial_\mu K^+\Lambda^{*\mu}, \tag{A6}$$

$$\mathcal{L}_{\gamma K\phi N} = i\frac{e g_{KN\Lambda^*}}{m_K}\bar{N}\gamma_5 K^+\Lambda^{*\mu}A_\mu. \tag{A7}$$

Coupling constants are shown in Table II.

In the amplitudes calculated from the above Lagrangians, we have used the form factor

$$F_x = \frac{\Lambda_c^4}{\left(x - m_x^2\right)^2 + \Lambda_c^4}, \qquad x = s, t, u, \tag{A8}$$

where Λ_c is the cutoff. We take the cutoff $\Lambda_c = 1.2$ GeV for ground state hadrons and $\Lambda_c = 0.7$ GeV for the $\Lambda(1520)$ resonance. To satisfy gauge invariance, we follow the suggestion of Davidson and Workman [28],

$$\begin{aligned}\mathcal{F}\mathcal{M} = {} & F_s\mathcal{M}_{s,\circ} + F_u\mathcal{M}_{u,\circ} + F_t\mathcal{M}_{t,\circ} \\ & + F_c(\mathcal{M}_{s,\times} + \mathcal{M}_{u,\times} + \mathcal{M}_{t,\times} + \mathcal{M}_c),\end{aligned}$$

where $\mathcal{M}_{x,\circ}$ is the gauge invariant part of the x-channel amplitude and $\mathcal{M}_{x,\times}$ is not. Here F_c is defined as

$$F_c = 1 - (1 - F_s)(1 - F_u)(1 - F_t). \tag{A9}$$

We use this procedure for the $\gamma N \to K\Lambda(1520)$ kernel. For the $\phi N \to K\Lambda(1520)$ kernel, all born contributions are multiplied by the form factor F_c. For the $\gamma N \to \phi N$ kernel, we follow Titov's approach [10].

APPENDIX B: DETERMINATION OF AN EFFECTIVE KAON WIDTH

To determine the effective width for the kaon exchanged in the transition $K\Lambda(1520) \to \phi N$, we express the intermediate kaon propagator as a function of the c.m. energy W and the angle θ_K between the out-going ϕ meson and in-coming kaon. The left-hand side of Eq. (17) can be described as

$$\begin{aligned} g_\phi(W,\cos\theta_K) &= \frac{i}{(p_\phi - p_K)^2 - m_{K_{\rm in}}^2 + i\epsilon} \\ &= \int dm_\phi^2\,\delta\left(m_\phi^2 - \bar{m}_\phi^2\right)\frac{i}{(p_\phi - p_K)^2 - m_{K_{\rm in}}^2 + i\epsilon}, \end{aligned}$$

where $\bar{m}_\phi$ is the physical ϕ-meson mass, $\bar{m}_\phi = 1.02$ GeV, and $m_{K_{\rm in}}$ is the exchanged kaon mass. By using a smearing function, we introduce the physical ϕ-meson width Γ_ϕ

$$\begin{aligned} g_\phi(W,\cos\theta) \to {} & \int dm_\phi^2 f\left(m_\phi^2 - \bar{m}_\phi^2, \Gamma_\phi\right) \\ & \times \frac{i}{(p_\phi - p_K)^2 - m_{K_{\rm in}}^2 + i\epsilon}, \end{aligned}$$

where the smearing function f is given by the imaginary part of the ϕ-meson propagator

$$f\left(m_\phi^2 - \bar{m}_\phi^2, \Gamma_\phi\right) = \frac{\bar{m}_\phi\Gamma_\phi}{\left(m_\phi^2 - \bar{m}_\phi^2\right)^2 + \bar{m}_\phi^2\Gamma_\phi^2}.$$

When the exchanged kaon reaches the on-shell point, the propagator is given by

$$\begin{aligned} g_\phi(W,\cos\theta) \to {} & \int dm_\phi^2 f\left(m_\phi^2 - \bar{m}_\phi^2, \Gamma_\phi\right) \\ & \times i[-i\delta(D(\cos\theta, m_\phi))], \end{aligned}$$

where the function $D(\cos\theta, m_\phi)$ is defined by

$$D(\cos\theta, m_\phi) = \cos\theta - F(m_\phi).$$

Here the function $F(m_\phi)$ is given by

$$F(m_\phi) = \frac{2E_\phi E_K - m_\phi^2}{2|\vec{p}_\phi||\vec{p}_K|}, \tag{B1}$$

where $\vec{p}_\phi$ and $\vec{p}_K$ are the three-momentum vector of the ϕ meson and the out-going kaon, respectively. We perform the integral, giving

$$\begin{aligned} g_\phi(W,\cos\theta) &= \int \frac{dm_\phi^2}{dF} dF f(m_\phi - \bar{m}_\phi, \Gamma_\phi) \\ &\quad \times i(-i)\delta(\cos\theta - F(m_\phi)) \\ &= \left(\frac{dF}{dm_\phi^2}\right)^{-1}_{m_\phi^2 = m_\phi'^2} f\left(m_\phi'^2 - \bar{m}_\phi^2, \Gamma_\phi\right). \end{aligned}$$

The introduced mass m'_ϕ denotes the solution of the equation $D(\cos\theta, m'_\phi) = 0$ and is a function of $\cos\theta$. Along the same lines, one can also introduce the $\Lambda(1520)$ resonance width Γ_{Λ^*} in the picture,

$$\begin{aligned} g_{\Lambda^*}(W,\cos\theta) &= \int \frac{dm_{\Lambda^*}^2}{dF} dF f\left(m_{\Lambda^*}^2 - \bar{m}_{\Lambda^*}^2, \Gamma_{\Lambda^*}\right) \\ &\quad \times i(-i)\delta(\cos\theta - F(m_{\Lambda^*})) \\ &= \left(\frac{dF}{dm_{\Lambda^*}^2}\right)^{-1}_{m_{\Lambda^*}^2 = m_{\Lambda^*}'^2} f\left(m_{\Lambda^*}'^2 - \bar{m}_{\Lambda^*}^2, \Gamma_{\Lambda^*}\right), \end{aligned}$$

where the mass m'_{Λ^*} denotes the solution of the equation $\cos\theta - F(m'_{\Lambda^*}) = 0$. Finally we introduce the effective kaon width as

$$\begin{aligned} g_{K_{\rm in}}(W,\cos\theta) &= \int \frac{dm_{K_{\rm in}}^2}{dF} dF f\left(m_{K_{\rm in}}^2 - \bar{m}_{K_{\rm in}}^2, \Gamma_{K_{\rm in}}\right) \\ &\quad \times i(-i)\delta(\cos\theta - F(m_{K_{\rm in}})) \\ &= \left(\frac{dF}{dm_{K_{\rm in}}^2}\right)^{-1}_{m_{K_{\rm in}}^2 = m_{K_{\rm in}}'^2} f\left(m_{K_{\rm in}}'^2 - \bar{m}_{K_{\rm in}}^2, \Gamma_{K_{\rm in}}\right), \end{aligned}$$

where the mass $m'_{K_{\rm in}}$ refers to a solution of the equation $\cos\theta - F(m_{K_{\rm in}}) = 0$, and the function F is defined as

$$F(m_{K_{\rm in}}) = \frac{2E_\phi E_K - m_\phi^2 + \left(m_{K_{\rm in}}^2 - \bar{m}_K^2\right)}{2|\vec{p}_\phi||\vec{p}_K|}. \tag{B2}$$

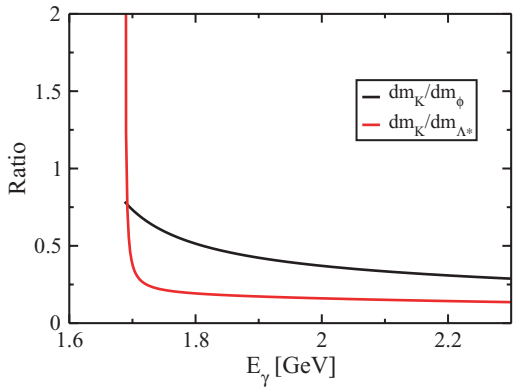

FIG. 12. (Color online) Ratio of the widths given by Eqs. (B3) and (B4).

We can obtain the ratio of the effective width of the intermediate kaon $K_{\rm in}$ and the widths of the ϕ meson or the Λ^* resonance from dF/dm_x, where x denotes ϕ, Λ^*, or $K_{\rm in}$,

$$\frac{(dF/dm_\phi)|_{m_\phi=\bar{m}_\phi}}{(dF/dm_{K_{\rm in}})|_{m_{K_{\rm in}}=\bar{m}_{K_{\rm in}}}} = \frac{dm_{K_{\rm in}}}{dm_\phi} = \frac{\Gamma_{K_{\rm in}}}{\Gamma_\phi}, \tag{B3}$$

and

$$\frac{(dF/dm_{\Lambda^*})|_{m_{\Lambda^*}=\bar{m}_{\Lambda^*}}}{(dF/dm_{K_{\rm in}})|_{m_{K_{\rm in}}=\bar{m}_{K_{\rm in}}}} = \frac{dm_{K_{\rm in}}}{dm_{\Lambda^*}} = \frac{\Gamma_{K_{\rm in}}}{\Gamma_{\Lambda^*}}. \tag{B4}$$

Figure 12 shows $dm_{K_{\rm in}}/dm_\phi$ and $dm_{K_{\rm in}}/dm_{\Lambda^*}$ as functions of the photon energy E_γ.

Substituting the physical widths of the ϕ meson $\Gamma_\phi = 4.26$ MeV and the $\Lambda(1520)$ resonance $\Gamma_{\Lambda^*} = 15.6$ MeV, we obtain from Fig. 12 the corresponding kaon width at $E_\gamma = 1.77$ GeV,

$$\Gamma^\phi_{K_{\rm in}} = \frac{dm_{K_{\rm in}}}{dm_\phi}\Gamma_\phi = 4.97 \text{ MeV},$$
$$\Gamma^{\Lambda^*}_{K_{\rm in}} = \frac{dm_{K_{\rm in}}}{dm_{\Lambda^*}}\Gamma_{\Lambda^*} = 9.87 \text{ MeV},$$

at $E_\gamma = 2.1$ GeV (the end of blue region), we obtain

$$\Gamma^\phi_{K_{\rm in}} = \frac{dm_{K_{\rm in}}}{dm_\phi}\Gamma_\phi = 2.94 \text{ MeV},$$
$$\Gamma^{\Lambda^*}_{K_{\rm in}} = \frac{dm_{K_{\rm in}}}{dm_{\Lambda^*}}\Gamma_{\Lambda^*} = 7.23 \text{ MeV}.$$

The functions g are displayed at $E_\gamma = 1.77$ GeV in Fig. 13, and for $E\gamma = 2.1$ GeV in Fig. 14. These figures show that $g_{K_{\rm in}}(\cos\theta)$ is in good agreement with $g_\phi(\cos\theta)$ and $g_{\Lambda^*}(\cos\theta)$. This means that the effective width of the intermediate kaon can accurately account for the physical decay width of the ϕ meson and the $\Lambda(1520)$ resonance. We define the effective intermediate kaon width Γ_K as

$$\Gamma_K = \sqrt{\Gamma^{\phi 2}_K + \Gamma^{\Lambda^* 2}_K}. \tag{B5}$$

Typical values for Γ_K are, for example,

$$\Gamma_K = 11.1 \text{ MeV} \quad \text{at} \quad E_\gamma = 1.77 \text{ GeV},$$
$$\Gamma_K = 7.79 \text{ MeV} \quad \text{at} \quad E_\gamma = 2.1 \text{ GeV}.$$

APPENDIX C: RARITA-SCHWINGER VECTOR SPINOR

We can decompose the Rarita-Schwinger vector spinor [29] for the different spin states as follows:

$$u^\mu(p, 3/2) = e^\mu_+(p)u(p, 1/2),$$
$$u^\mu(p, 1/2) = \sqrt{\frac{2}{3}}e^\mu_0(p)u(p, 1/2) + \sqrt{\frac{1}{3}}e^\mu_+(p)u(p, -1/2),$$
$$u^\mu(p, -1/2) = \sqrt{\frac{1}{3}}e^\mu_-(p)u(p, 1/2) + \sqrt{\frac{2}{3}}e^\mu_0(p)u(p, -1/2),$$
$$u^\mu(p, -3/2) = e^\mu_-(p)u(p, -1/2).$$

Here we use the basis four-vectors e^μ_λ, which are given as

$$e^\mu_\lambda(p) = \left(\frac{\vec{\epsilon}_\lambda \cdot \vec{p}}{M_B}, \epsilon_\lambda + \frac{\vec{p}(\vec{\epsilon}_\lambda \cdot \vec{p})}{M_B(p^0 + M_B)}\right)$$

with

$$\vec{\epsilon}_+ = -\frac{1}{\sqrt{2}}(1, i, 0), \quad \vec{\epsilon}_0 = (0, 0, 1), \quad \vec{\epsilon}_- = \frac{1}{\sqrt{2}}(1, -i, 0).$$

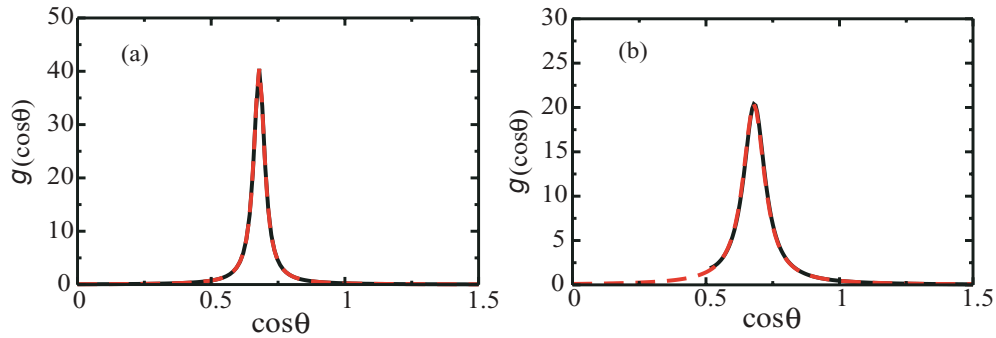

FIG. 13. (Color online) On-shell exchanged kaon propagator at $E_\gamma = 1.77$ GeV as a function of angle. (a) Black solid line denotes $g_\phi(\cos\theta)$ with the physical ϕ-meson width Γ_ϕ, and the dashed line is $g_K(\cos\theta)$ with the corresponding kaon width $\Gamma^\phi_K = 4.97$ MeV. (b) Black solid line is $g_{\Lambda^*}(\cos\theta)$ with the physical $\Lambda(1520)$ width $\Gamma_{\Lambda(1520)}$, and the dashed line is $g_K(\cos\theta)$ with the corresponding kaon width $\Gamma^{\Lambda^*}_K = 9.87$ MeV.

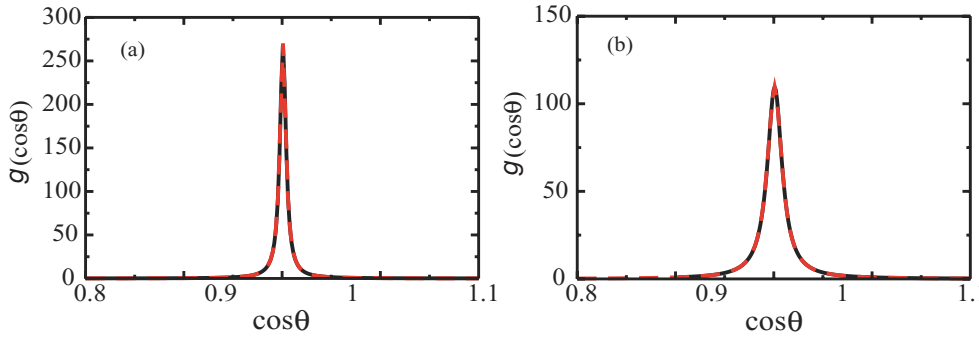

FIG. 14. (Color online) On-shell exchanged kaon propagator at $E_\gamma = 2.1$ GeV as a function of angle. (a) Black solid line is $g_\phi(\cos\theta)$ with the physical ϕ width Γ_ϕ, and the dashed line is $g_K(\cos\theta)$ with the corresponding kaon width $\Gamma_K^\phi = 2.94$ MeV. (b) Black solid line is $g_{\Lambda^*}(\cos\theta)$ with the physical $\Lambda(1520)$ width $\Gamma_{\Lambda(1520)}$, and the dashed line is $g_K(\cos\theta)$ with the corresponding kaon width $\Gamma_K^{\Lambda^*} = 7.23$ MeV.

APPENDIX D: SPIN-DENSITY MATRIX

In terms of helicity amplitudes $T_{\lambda_f,\lambda;\lambda_i,\lambda_\gamma}$, spin-density matrices can be written as [11,26]

$$\rho^0_{\lambda\lambda'} = \frac{1}{N}\sum_{\lambda_\gamma,\lambda_i,\lambda_f} T_{\lambda_f,\lambda;\lambda_i,\lambda_\gamma}\, T^*_{\lambda_f,\lambda';\lambda_i,\lambda_\gamma}, \tag{D1}$$

$$\rho^1_{\lambda\lambda'} = \frac{1}{N}\sum_{\lambda_\gamma,\lambda_i,\lambda_f} T_{\lambda_f,\lambda;\lambda_i,-\lambda_\gamma}\, T^*_{\lambda_f,\lambda';\lambda_i,\lambda_\gamma}, \tag{D2}$$

$$\rho^2_{\lambda\lambda'} = \frac{i}{N}\sum_{\lambda_\gamma,\lambda_i,\lambda_f} \lambda_\gamma T_{\lambda_f,\lambda;\lambda_i,-\lambda_\gamma}\, T^*_{\lambda_f,\lambda';\lambda_i,\lambda_\gamma}, \tag{D3}$$

$$\rho^3_{\lambda\lambda'} = \frac{1}{N}\sum_{\lambda_\gamma,\lambda_i,\lambda_f} \lambda_\gamma T_{\lambda_f,\lambda;\lambda_i,\lambda_\gamma}\, T^*_{\lambda_f,\lambda';\lambda_i,\lambda_\gamma}, \tag{D4}$$

where

$$N = \sum |T_{\lambda_f,\lambda;\lambda_i,\lambda_\gamma}|^2. \tag{D5}$$

Here the helicities λ_γ, λ_i, and λ_f are for the photon and initial and final nucleons, while λ and λ' are for the ϕ meson. To calculate the spin-density matrix in the GJ system, one needs a transformation from the c.m. to the GJ system. This transformation is done in terms of

$$T^{\rm GJ}_{\lambda_f,\lambda\phi;\lambda_i,\lambda_\gamma} = \sum_{l,m} T^{\rm c.m.}_{\lambda_f l;m\lambda_\gamma} d^1_{l\lambda}(-\omega_\phi)\, d^{1/2}_{m\lambda_i}(-\omega_p), \tag{D6}$$

where the corresponding Wigner rotating angles are given by

$$\omega_\phi = \text{acos}\left(\frac{\cos\theta - u_\phi}{1 - u_\phi\cos\theta}\right), \tag{D7}$$

$$\omega_p = \text{atan}\left(\frac{u_\phi \sin(\pi-\theta)(1-v_p^2)^{1/2}}{v_p + u_\phi\cos(\pi-\theta)}\right). \tag{D8}$$

Here θ is the angle of the outgoing ϕ meson in the c.m. system, while v_p and u_ϕ are the proton and the ϕ-meson velocities in the c.m. system, respectively.

[1] T. Nakano *et al.* (LEPS Collaboration), Phys. Rev. Lett. **91**, 012002 (2003).
[2] T. Nakano *et al.* (LEPS Collaboration), Phys. Rev. C **79**, 025210 (2009).
[3] S. P. Barrow *et al.* (CLAS Collaboration), Phys. Rev. C **64**, 044601 (2001).
[4] M. Niiyama *et al.*, Phys. Rev. C **78**, 035202 (2008).
[5] E. Anciant *et al.* (CLAS Collaboration), Phys. Rev. Lett. **85**, 4682 (2000).
[6] T. Mibe *et al.* (LEPS Collaboration), Phys. Rev. Lett. **95**, 182001 (2005).
[7] J. P. Santoro *et al.* (CLAS Collaboration), Phys. Rev. C **78**, 025210 (2008).
[8] Durham database, http://www.slac.stanford.edu/spires/hepdata/.
[9] A. I. Titov and T. S. H. Lee, Phys. Rev. C **67**, 065205 (2003).
[10] A. I. Titov and B. Kampfer, Phys. Rev. C **76**, 035202 (2007).
[11] A. I. Titov, T. S. H. Lee, H. Toki, and O. Streltsova, Phys. Rev. C **60**, 035205 (1999).
[12] S. I. Nam, A. Hosaka, and H. C. Kim, Phys. Rev. D **71**, 114012 (2005).
[13] A. Y. Korchin, O. Scholten, and R. G. E. Timmermans, Phys. Lett. **B438**, 1 (1998).
[14] A. Usov and O. Scholten, Phys. Rev. C **72**, 025205 (2005).
[15] O. Scholten, S. Kondratyuk, L. Van Daele, D. van Neck, M. Waroquier, and A. Y. Korchin, Acta Phys. Pol. B **33**, 847 (2002).
[16] A. Donnachie and P. V. Landshoff, Phys. Lett. **B185**, 403 (1987).
[17] N. Muramatsu *et al.*, Phys. Rev. Lett. **103**, 012001 (2009).
[18] D. P. Barber *et al.*, Z. Phys. C **7**, 17 (1980).
[19] Y. Kanada-En'yo and D. Jido, Phys. Rev. C **78**, 025212 (2008).
[20] D. Jido and Y. Kanada-En'yo, Phys. Rev. C **78**, 035203 (2008).
[21] A. Usov and O. Scholten, Phys. Rev. C **74**, 015205 (2006).
[22] M. Guidal, J. M. Laget, and M. Vanderhaeghen, Nucl. Phys. **A627**, 645 (1997).
[23] T. Corthals, J. Ryckebusch, and T. Van Cauteren, Phys. Rev. C **73**, 045207 (2006).
[24] T. Mart and C. Bennhold, arXiv:nucl-th/0412097.
[25] H. Toki, C. Garcia-Recio, and J. Nieves, Phys. Rev. D **77**, 034001 (2008).
[26] K. Schilling, P. Seyboth, and G. E. Wolf, Nucl. Phys. **B15**, 397 (1970); **B18**, 332 (1970).
[27] S. Ozaki, H. Nagahiro, and A. Hosaka, Phys. Lett. **B665**, 178 (2008).
[28] R. M. Davidson and R. Workman, Phys. Rev. C **63**, 058201 (2001).
[29] W. Rarita and J. Schwinger, Phys. Rev. **60**, 61 (1941).